



Physicochemical characterization and catalytic performance of Fe doped CuS thin films deposited by the chemical spray pyrolysis technique

M. Rouchdi¹ · H. Mamori² · E. Salmani² · B. Ait Syad² · O. Mounkachi^{2,5} · R. Essajai¹ · H. Ez-zahraouy² · H. Chakchak⁴ · N. Hassanain¹ · A. Benyoussef³ · A. El Kenz² · A. Mzerd¹

Received: 23 February 2021 / Accepted: 9 May 2021 / Published online: 22 May 2021
© The Author(s), under exclusive licence to Springer-Verlag GmbH, DE part of Springer Nature 2021

Abstract

The thin films Fe doped copper sulphide $\text{Cu}_{1-x}\text{Fe}_x\text{S}$ (CFS) ($x = 0.01, 0.03, 0.05,$ and 0.07) were elaborated by spray pyrolysis deposition technique. The characterization by XRD and SEM of the thin films shows a Covellite CuS single phase without formation of other phases. The structure is a simple hexagonal with unit cell dimension, $a = b = 3.79 \text{ \AA}$ and $c = 16.34 \text{ \AA}$. The Analysis of the UV–Vis spectra reveals that the energy band gap has been decreased from 2.47 to 1.98 eV with the increase of Fe concentration. The absorption coefficients of CFS films have increased from 1.155×10^5 to $1.712 \times 10^5 \text{ cm}^{-1}$. It has demonstrated that a right band gap with a right band edge alignment at a pH value for Fe-doped CFS can boost the material application as a photocatalyst for the visible light. According to this study, CFS (0.07) thin films for a pH = 3 solutions is a promising material for photocatalysis application for water splitting to hydrogen-oxygen production. Nevertheless, we demonstrate that the formation of straddling gap heterostructure for CuS and CFS for a pH solution between 7 and 8 induces the production of oxygen and hydrogen.

Keywords CuS · Thin films · CFS · Spray pyrolysis · Hydrogen–oxygen production · Photocatalysis · Optical properties

1 Introduction

A photocatalyst is defined as a process based on a semiconductor material when a photocatalyst semiconductor is irradiated by light, the absorbing light; create electron–hole pairs by electronic transitions. The photocatalyst semiconductor triggers through this pairs a reduction and/or an oxidation reaction. The photocatalytic system has several characteristics, including the band gap, the position of the upper edge of valence band (VB), and the lower edge of the conduction band (CB), in comparison to water oxidation–reduction potential, in which the VB should locate more negative to the oxidizing potential, and the CB should locate more positive to the reducing potential. There are many photocatalysts reported in the literature [1–7]. The most studied and commercially used are metal oxides like, TiO_2 , ZnO and SnO_2 , elements that are much available in nature and stable in different of conditions. However, it can absorb ultraviolet light and can exploit just 3% to 5% of the solar spectrum energy due to the band gap energy range between 3.2 and 3.68 eV. Considerable strategies have been developed to improve the absorption performance to utilize

✉ M. Rouchdi
rouchdi.mus@gmail.com

E. Salmani
elmehdisalmani@gmail.com

¹ Centre de Recherche en Énergie–Équipe des semi-conducteurs et technologie des capteurs d’environnement (STCE), Faculty of Science, Mohammed V University, B.P. 1014, Rabat, Morocco

² Laboratoire de la Matière Condensée et Sciences Interdisciplinaires (LaMCSi), Faculty of Science, Mohammed V University, B.P. 1014, Rabat, Morocco

³ Materials and Nanomaterials Centre, Moroccan Foundation for Advanced Science, Innovation and Research, MAScIR, Rabat, Morocco

⁴ Unités d’Appui Techniques à la Recherche Scientifique au Centre National pour la Recherche Scientifique et Technique (UATRS–CNRST), B.P. 8027 N.U., 10102 Rabat, Morocco

⁵ MSDA, Mohammed VI Polytechnic University, Lot 660, Hay Moulay Rachid, 43150 Ben Guerir, Morocco

the solar spectrum more efficiently, such as heterojunction structures [1, 2]. Recently, a new family of materials based on chalcogenides has been developed; possess smaller band gaps, which is favourable for visible-light absorption [3–8]. In this article, we thoroughly synthesis and study Covellite copper sulphide (CuS); It is one of the chalcogenide semiconductors. CuS crystallizes in a simple hexagonal structure forming the $P6_3/mmc(194)$ space group with lattice dimension, $a = 3.79 \text{ \AA}$ and $c = 16.36 \text{ \AA}$ [9]. The CuS has some particularities, as band gap energy of 2.36 eV [10], high conductivity and a good optical absorption coefficient [11, 12], besides it includes only the earth abundant elements, inexpensive, easy to prepare and non-toxic. It has also other fascinating physical and chemical properties (electronic, optical,...) which can be used in semiconductors [6, 13–15], and has great attention, due to the wide range variation of the stoichiometric composition including Cu_2S , Cu_7S_4 , $\text{Cu}_{1.94}\text{S}$, $\text{Cu}_{1.96}\text{S}$ and CuS [16, 17]. It has many potential applications for electrodes [18], solar energy conversion through photoelectron chemical cells [19], cathode of high-capacity material in lithium rechargeable batteries [20], application for a nonlinear optical materials, solar controller, solar radiation absorber [21], chemical sensors [22], catalyst [23], and thermoelectric cooling material [24]. Considering the different technological applications and various morphologies of CuS compound [25–31], that has been made by deposition techniques such as hydrothermal [32, 33], solvothermal [34, 35], thermolysis [36], microemulsion [37], chemical vapour deposition (CVD) [38], wet chemical method [39] or spray pyrolysis [40], etc. In order to enhance some physical properties notably optical and electrical, many recent researchers focus on doping copper sulphide with different elements as Zn or Pb [41, 42], which showed that after doping, the properties of CuS changed and kept different perspectives. For example, Ali Yildirim et al. [41] have used the SILAR method to investigate the physical characteristics of Zn doped CuS, and have showed that CuZnS has a hexagonal crystal structure, and they have exhibited that depending on Zn content the energy band gap can be increased from 2.03 to 2.14 eV and that with the increase of intensity of light, the current can be raised by the increasing rate of illuminated 500 W cm^{-2} films. By a simple chemical co-precipitation method, Sreelekha et al. [14] have noted too that the optical band-gap changes according to cobalt content. Suarez et al. [42] performed a detailed X-ray diffraction (XRD) aiming to elaborate the thin film and study his electrical characteristics for doping $(\text{PbS})_{1-x}(\text{CuS})_x$ films. They have shown the presence of PbS and traces of CuS in the films, with p-type conductivity behaviour. Besides that, a number of studies have focused on the properties of this material doping with some transition metals (Fe, Co, Ni) in view of a possible applications in photocatalytic [14, 15, 43]. In order to study the magnetic properties, other researchers have investigated

the dilute magnetic semiconductors (DMSs) which have a suitable band gap of the prevailing semiconductor and their strong ferromagnetism behaviour at room temperature through doping with other metallic elements (Cr, Mn, Fe, Co and Ni) intended for spintronic device application [44, 45]. More Recently, Sreelekha et al. [14] have also synthesized Fe doped (CFS) using chemical co-precipitation route and revealed that the transition from the ferromagnetic phase to the paramagnetic phase depends on the concentration of Fe doping CuS with strong ferromagnetism for 3% Fe doped CuS at room temperature. The aim of our work is to study the $(\text{Cu}_{1-x}\text{Fe}_x\text{S})$ thin films deposited evolution employing the chemical spray pyrolysis technique with optimizing application parameters such as host and dopant concentration, flow rate, time and distance of spraying, nature and pressure of carrier gas, as well as substrate temperature and solvents used. Such studies are not discussed in most of the available work on $\text{Cu}_{1-x}\text{Fe}_x\text{S}$ (CFS) thin films [18–45]. We have highlighted here, the variation of the band gap and the changes in the alignment of the edges band of the Fe doped CuS with different pH solutions. This study proves that with an appropriate Fe concentration, our thin films are an appropriate semiconductor with optical properties that promote its application as a visible light photocatalyst in hydrogen-oxygen production by water splitting.

2 Materials and methods

2.1 CFS thin film operating mode

As mentioned in our previous thin film research, $\text{Cu}_{1-x}\text{Fe}_x\text{S}$ thin films were sprayed onto soda–lime glass substrates (Dimensions, length \times width \times thickness: $1 \text{ cm} \times 1 \text{ cm} \times 0.1 \text{ cm}$ respectively) maintained at $500 \text{ }^\circ\text{C}$ using chemical spray pyrolysis technique (CSP) [46–51]. For a variation in the amount of FeCl_2 from 0.01 to 0.07 the concentration of CuCl_2 was 0.02 M and $\text{CS}(\text{NH}_2)_2$ was 0.08 M in solution. In the process of the homogeneous solution preparation, we used 5 ml of ethanol as solvent at room temperature, with solutions of iron chloride ($\text{FeCl}_2 \cdot 4\text{H}_2\text{O}$), copper chloride ($\text{CuCl}_2 \cdot 2\text{H}_2\text{O}$), and thiourea ($\text{CS}(\text{NH}_2)_2$) in 200 ml of distilled water. Then the solution is agitated for more than 40 min at $40 \text{ }^\circ\text{C}$. The use of the solvent improves the stability of the mixture and makes a better quality films. One of the most important steps before starting the process is to prepare soda–lime glass substrates is cleaning it from every particle of dirt with ethanol and distilled water for 15 min respectively before having it dry with a hairdryer, and checking if the surface of the substrate is perfectly flat without any scratches, we generally use the soda–lime glass substrates shaped by diamond to avoid flatness defects. Fig. 1 illustrates a schematic explanation

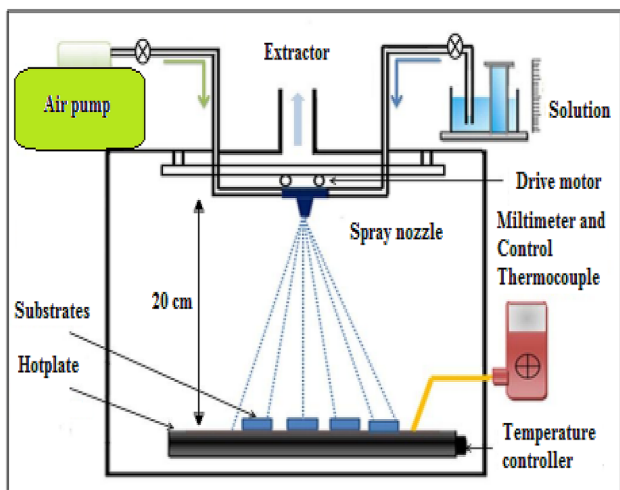


Fig. 1 Schematic of chemical spray pyrolysis technique (CSP)

of the chemical spray pyrolysis system. This system is made up of two major parts: the heating part, and the spraying part. The first one consists of the hotplate, the temperature controller and the thermocouple, the second one consist of the spray nozzle, the dosing pump and the drive motor. Referring to the Masterflex apparatus data the prepared solution was sprayed with a rate of 1.5 ml/min through the spray nozzle towards the substrates with about 40 μm droplets diameter, depending on the flow rate of the solution. The carrier gas of the sprayed the solution is the dry air. The samples of sprayed deposition have to be annealing for one hour at 500 °C.

2.2 The thin films characterization

To characterize the structure of thin films, we used the XRD system by a diffractometer (Bruker D8 Discover, Cu-Kα at λ = 0.154056 nm). To examine closely both the morphological and the chemical composition, we used an electron microscope (ZEISS EVO® MA 15). For the optical properties test of our thin films, we measured the electromagnetic spectrum from 300 to 800 nm including UV, visible and near infrared with a spectrophotometer (Lambda 900 UV/VIS/NIR).

3 Results and discussion

3.1 Structural properties

Figure 2 shows the X-ray diffraction results of the sprayed CuS and CFS thin films. The X-ray Diffraction results showed that CFS films crystallizes in the hexagonal phase with a privileged orientation along (102), these are well consistent with the JCPDS database standard (hexagonal phase, PDF no. 06-0464). For each value of peaks 23.4°, 23.44°, 27.88°, 29.4°, 31.8°, 48°, 52.76° and 57.12° can be attributed to (004), (100), (101), (102), (103), (110), (108) and (116) 57.12° planes respectively of CuS phase. The lattice dimensions are $a = 3.790 \text{ \AA}$ and $c = 16.370 \text{ \AA}$ that is harmony with the hexagonal type CuS structure [14]. The good dispersion and lower content of Fe doping no impurities peaks of such as Cu_xS and FeS have been observed in this pattern. The Fe doping's increase shifts slightly the (102) peak position of the simple towards a bigger diffraction

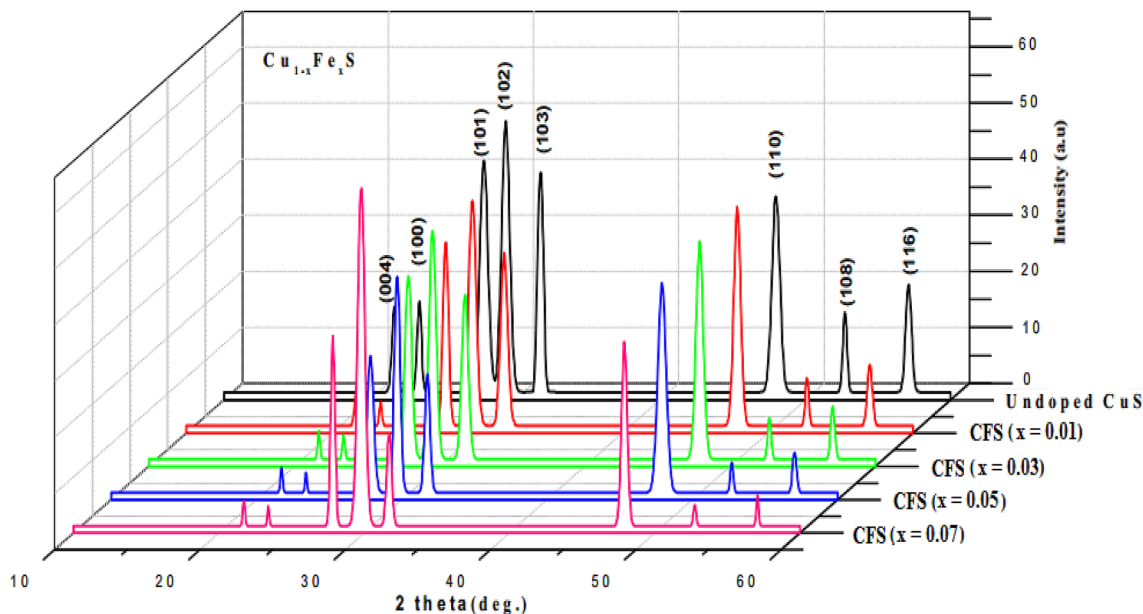


Fig. 2 X-ray diffraction pattern of undoped and various Fe-doped CuS thin films

angle. This due to the difference in the Fe^{2+} , Cu^{2+} radius (0.078 nm) and (0.065 nm), respectively, [43, 52]. Additionally to that, the variations of (102) high-flying peaks intensity meanwhile the FWHM changes, which might be attributed to incorporation of Fe^{2+} ion into Cu^{2+} site. For 0.01, 0.03 and 0.05 Fe-doped CuS thin films, their (102) peaks were gradually decreased, which could be attributed to an increase of stacking defects and a loss of periodicity in the deposition of CuS crystals. The increase in stacking faults as well as the loss of CuS crystals deposition periodicity. The film having the highest intensity is those attached to the 0.07 film concentration, subsequently, the best crystallization compared to the others films. This preferred orientation is explained of course by the start of a new nucleation in the proximity of doping atoms, thus promoting the development of CFS structure [52].

From Table 1, it is obvious that the increase in Fe doping causes lattice primitives expansion of a and c . So far, this result is clearly compatible with the expected result, because the radius of iron ions is larger than that of copper ions in CuS [43, 52]. Further, the average crystallite sizes were calculated in comparison using Debye-Scherrer and Williamson-Hall equations as Eqs. (1) and (2), respectively [48, 53]:

$$D = \frac{0,9\lambda}{\beta \cos \theta} \quad (1)$$

$$\beta \cos \theta = \frac{0,9\lambda}{D} + 4\varepsilon \sin \theta \quad (2)$$

With 0,9 is the shape factor, λ is the X-ray wavelength (equal to 0.15406 nm for $\text{CuK}\alpha$), β is the line broadening at half the maximum intensity (FWHM), θ is Bragg's angle and ε is the micro strain of the samples.

As shown in Table 1, the results of the calculated crystallite size were summarized from Scherrer's and Williamson-Hall formulae. The results of the Williamson-Hall analysis for the CuS and CFS thin films are shown in Fig. 3. Fit to the data, the strain is extracted from the slope and the crystalline size is extracted from the y-intercept of the fit.

According to Table 1, the calculated crystallites size of CFS was found to be in range of 121–171 Å due to improvement of its crystallinity, which is consistency with the reported studies [14, 15, 43]. At this point, the interpretation made by different authors is called that the FWHM decreases due to an increase in the crystal quality of the samples [54].

Also, it is obvious that the crystallite size calculated from XRD data using Scherrer equation is smaller than crystallite size determined from Williamson-Hall method. This might be due to the fact that the Scherrer method actually measures the coherence length of the X-rays, any crystal imperfections will cause the calculated size to be smaller than the true size but in WH method the microstrain effect was taken into consideration [55].

To calculate 'a' and 'c' lattice constants, we use the following equation [47]:

$$\frac{1}{d^2(hkl)} = \frac{h^2 + k^2}{a^2} + \frac{l^2}{c^2} \quad (3)$$

The surface morphology, density, shape and the crystallites distribution are well exposed by the electronic scanning microscopy analysis. Morphologies of the synthesized films for Fe concentrations are revealed in Fig. 4. We can establish that the films CuS and CFS crystallize in a hexagonal plate-like morphology, with an average thickness of about 400 nm, according to profilometer measurements. These conform well to XRD analysis. However, the observed surface morphology of the thin films shows a very well crystals growth with a good crystallinity. It is observed an important modification in morphology of the Fe doped CuS films as Fe dopant concentration was increased. This tendency can be caused by incorporation of Fe on the growing surface. The small growth shows that they are homogeneous without split or emptiness.

The typical EDX spectrum of deposited thin films is indicated in Fig. 4. The elementary analysis gave peaks indicating the presence of copper (Cu), sulphur (S) and iron (Fe) as well as other peaks indicating other elements such as Si(K), C(K) and Ca(K) have attributed to the soda-lime glass substrate.

Table 1 Structural parameters of undoped and various Fe-doped CuS thin films

Fe concentration (at%)	2θ value (Degree)	Full width half maxima (FWHM) (2θ Degree)	Average crystal size williamson-hall (D) (Å)	Average crystal size scherrer (D) (Å)	Cell parameter (Å)	
					$a = b$	c
Undoped CuS	29.52	0.65	163	121	3.790	16.370
$x = 0.01$	29.67	0.60	179	132	3.794	16.355
$x = 0.03$	29.67	0.58	185	136	3.797	16.370
$x = 0.05$	29.73	0.57	194	137	3.798	16.377
$x = 0.07$	29.79	0.46	219	171	3.805	16.385

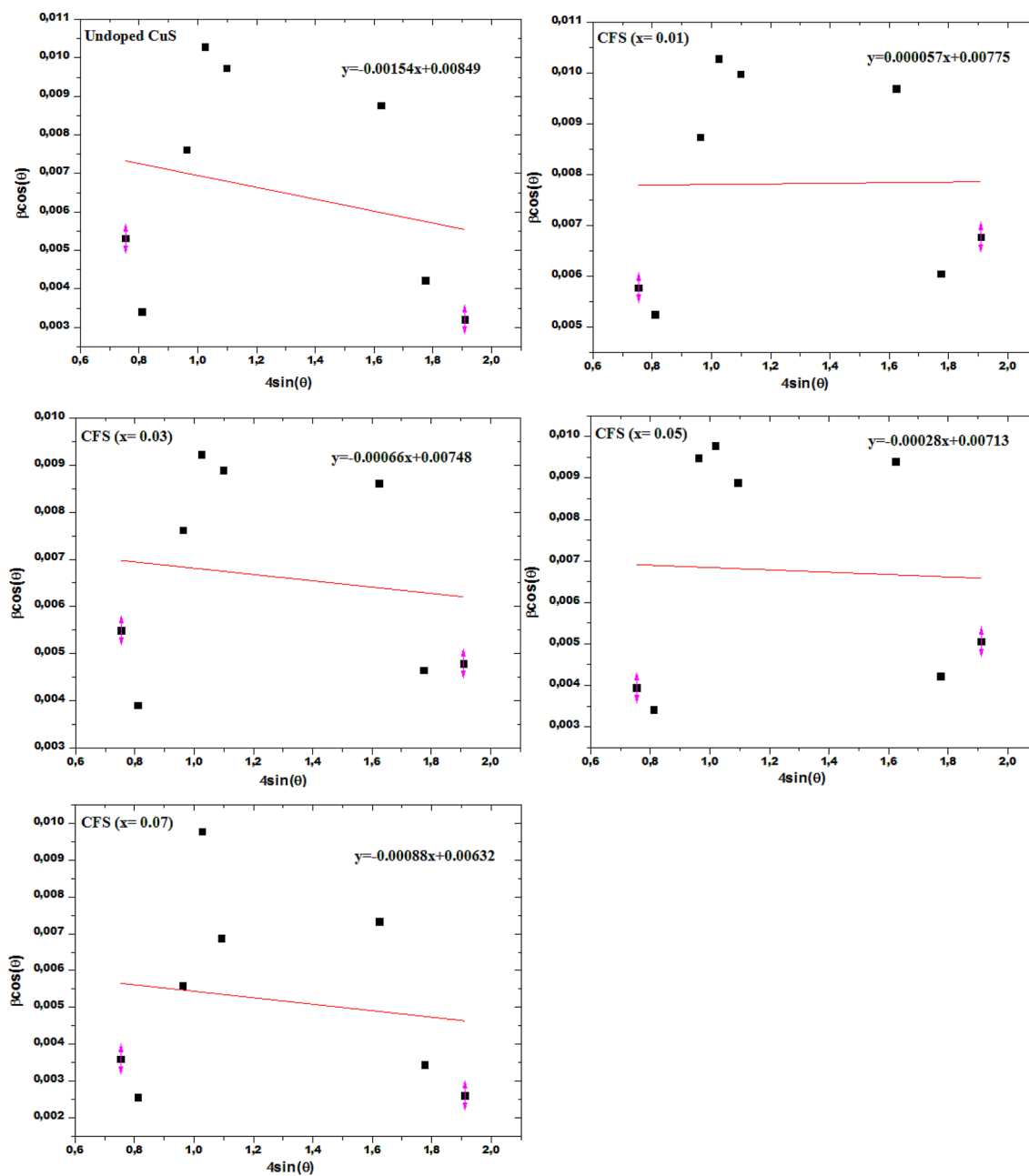


Fig. 3 The W–H plot of undoped and various Fe-doped CuS thin films

3.2 Optical properties

Figure 5 indicates the absorbance analysis in range the measuring from 300 to 800 nm. The results show that the samples exhibit a high absorbance in the visible region and the maximum value (2.9) was observed for 0.07. As illustrated in this figure, the wavelength of 350–600 nm represents the high absorption range of the films. It increases with increasing Fe doping, which demonstrates that Fe doped CuS thin films allows to absorb more radiation in this region as observed in previous studies [14, 15]. This strong

photonic excitation gives rise to an electronic transition of the valence band which is totally filled towards the conduction band. The result is electron/hole pairs (e^-/h^+) creation in the Fe-doped CuS that could initiate oxidation-reduction reactions for water splitting when exposure to air, or when it is in solutions. Using Tauc’s model Eq. (4), we estimated the energy band gap [49, 50]:

$$(ahv)^2 = A(hv - E_g) \tag{4}$$

Fig. 4 SEM images and EDX results of undoped and various Fe-doped CuS thin films

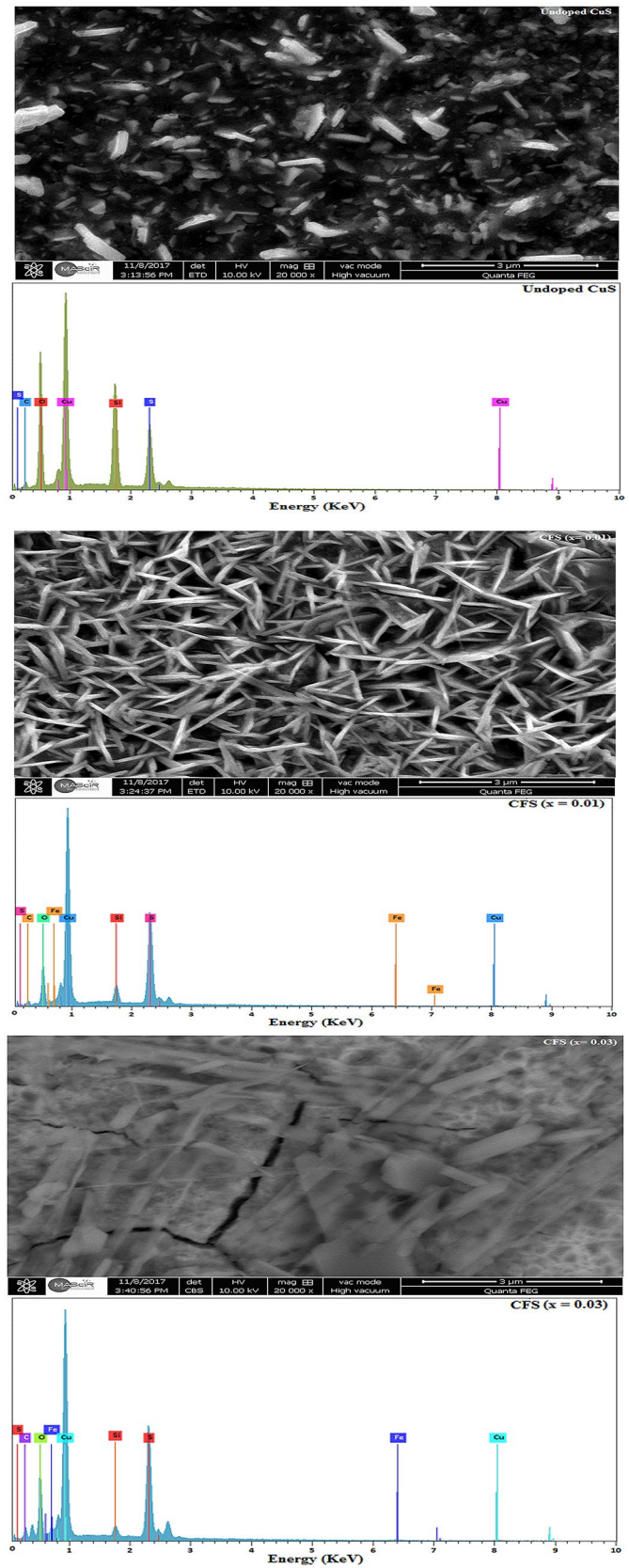


Fig. 4 (continued)

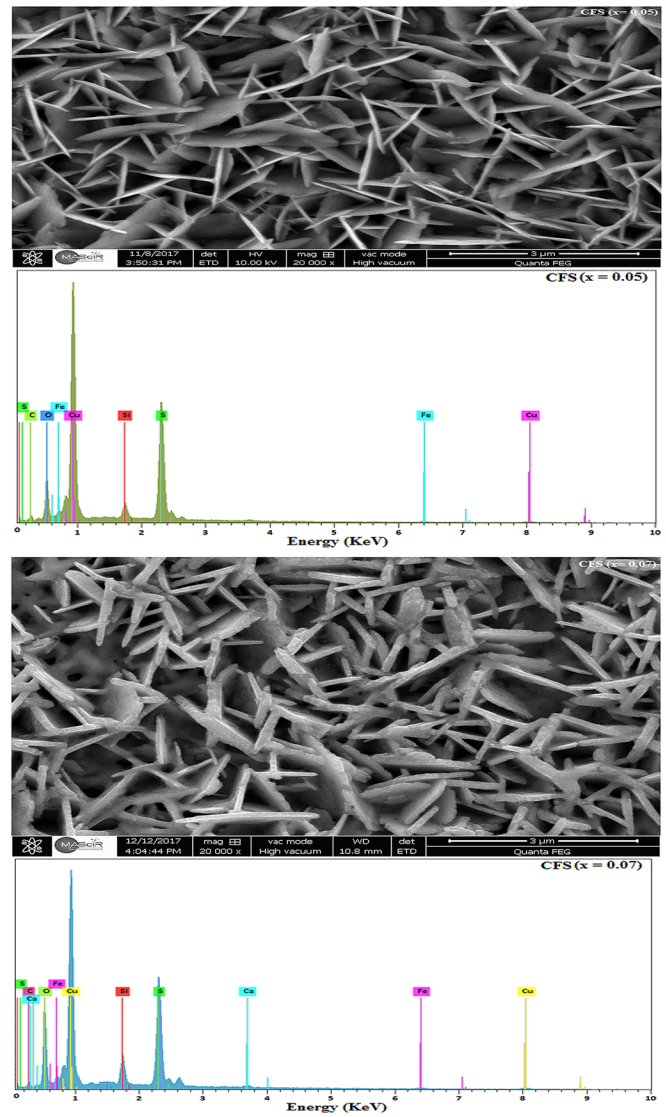
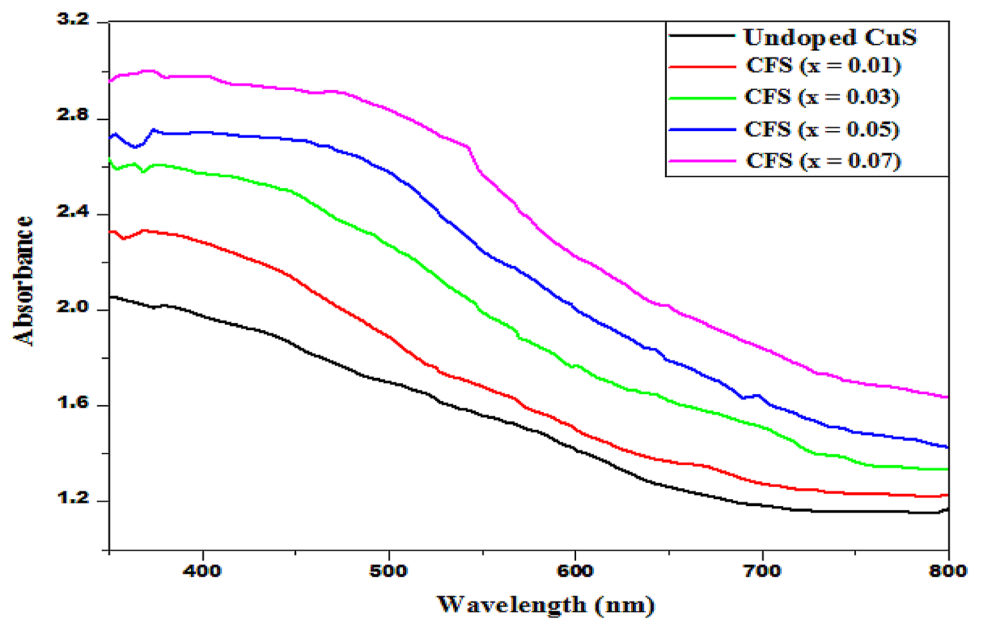


Fig. 5 Optical absorbance spectra of undoped and various Fe-doped CuS thin films



Where α is absorption coefficient, A is the constant related to the effective mass associated with the bands, E_g is the energy band gap, h is Planck’s constant, and ν is frequency.

The pure CuS and CFS thin films direct band gap was obtained by intercepting the curve linear regions between $h\nu$ and $(\alpha h\nu)^2$ illustrated in Fig. 6. For undoped CuS, the obtained direct band gap value is 2.47 eV. For doped $Cu_{1-x}Fe_xS$ (x s= 0.01, 0.03, 0.05 and 0.07) thin films, the measured band gap values are 2.34, 2.16, 1.99 and 1.98 eV respectively (Fig. 6). Here, the energy band gap values found near to the E_g values in a previous accounted study [14, 56, 57]. It has been found that the absorption edge changes with increasing Fe concentration, which stimulates a variation in the band gap value. The reasons explaining the narrowing values of band gap in thin films of semiconductors are reported here. This band gap reduction is due to the $sp-d$ exchange interaction of band electrons and Fe^{2+} localized electrons caused by the inclusion of Cu^{2+} sites [14]. Hence, the $s-d$ and $p-d$ interactions adjust positively and negatively the limits of conduction and valence bands (CB&VB), making a reduction of the band gap.

Further, this energy reduction may be explained by the carrier concentration enhancement by Fe ions inclusion and the generation of energy level traps in the host matrix band

gap [14]. Nonetheless, compared to TiO_2 , the CFS compound has the advantages, such as non-toxic, abundantly available in the earth’s crust and also with a very low cost, and we have demonstrated that the absorption can tune to the visible region with varying Fe concentration. Consequently, this ternary material could principally be developed as an efficient absorber semiconductor to enhance the photocatalytic activity.

Optical absorption spectra and Lambert’s law [58] allows the absorption coefficient α calculating of pure thin films CuS and CFS by the relation:

$$\ln\left(\frac{I}{I_0}\right) = 2.303A = \alpha t \tag{5}$$

with I_0 is the incident light intensity, I is the transmitted light intensity, t is the film thickness and A is the optical absorbance.

Figure 7 shows the absorption coefficient as a function of photon energy of Covellite CuS and CFS thin films with different Fe contents. It has been noticed that for the visible spectral range of ($> 10^5\text{ cm}^{-1}$), all the films exhibits a high absorption coefficient. Figure 7 shows that the absorption coefficients rise from 1.155×10^5 to

Fig. 6 Energy band gap of undoped and various Fe-doped CuS thin films

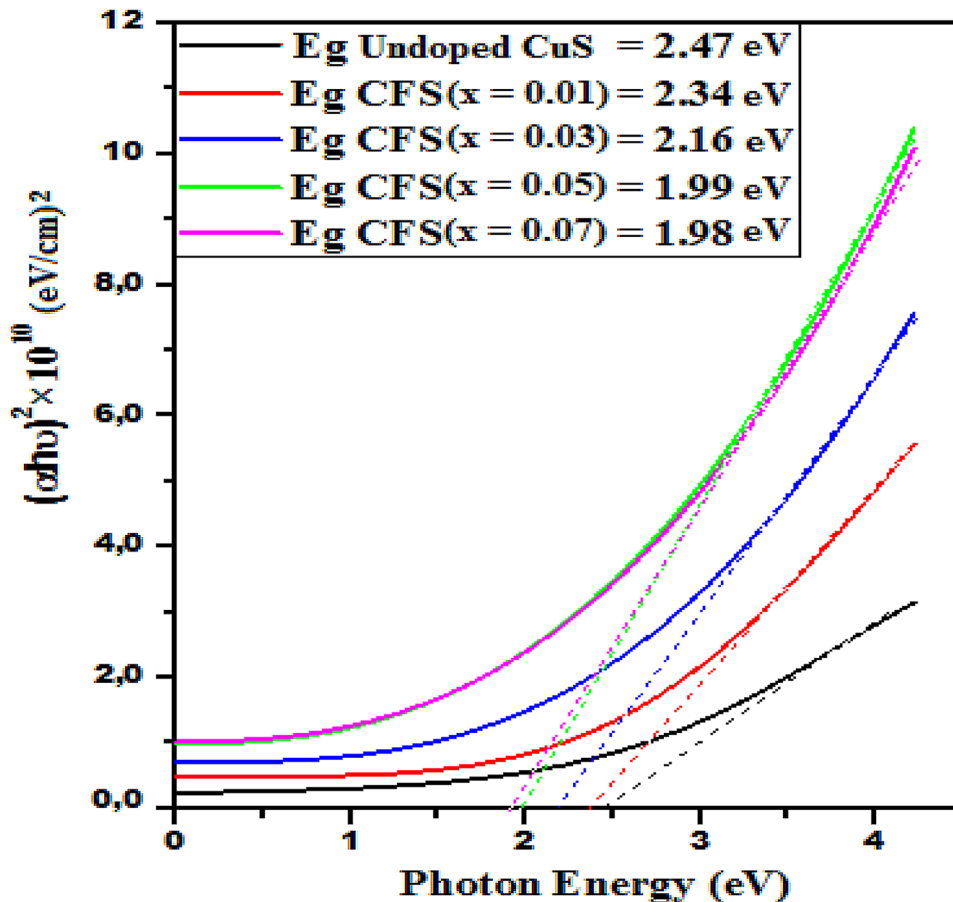
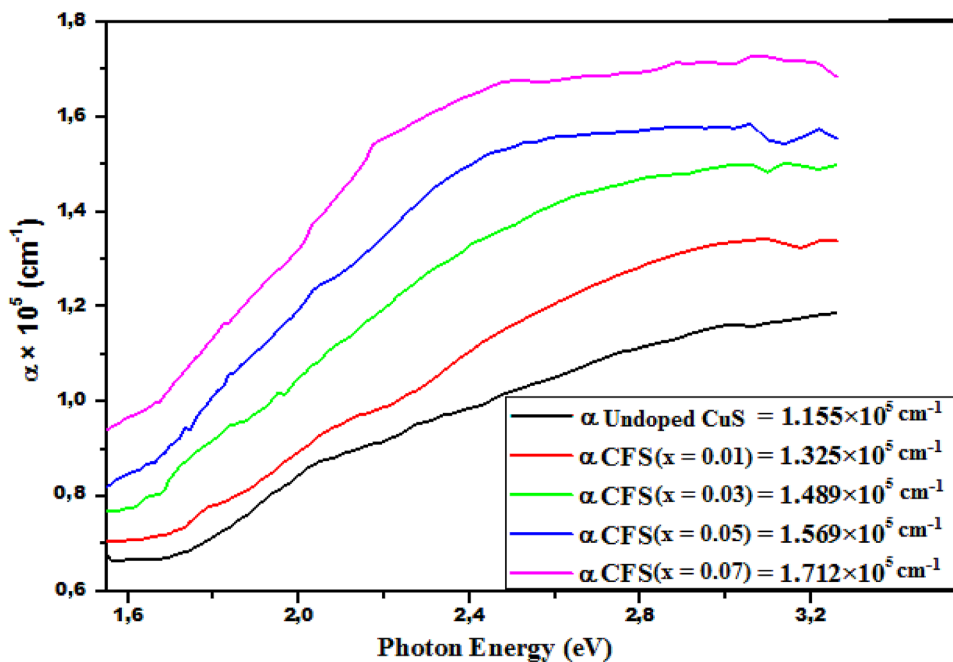


Fig. 7 Optical absorption coefficients of undoped and various Fe-doped CuS thin films

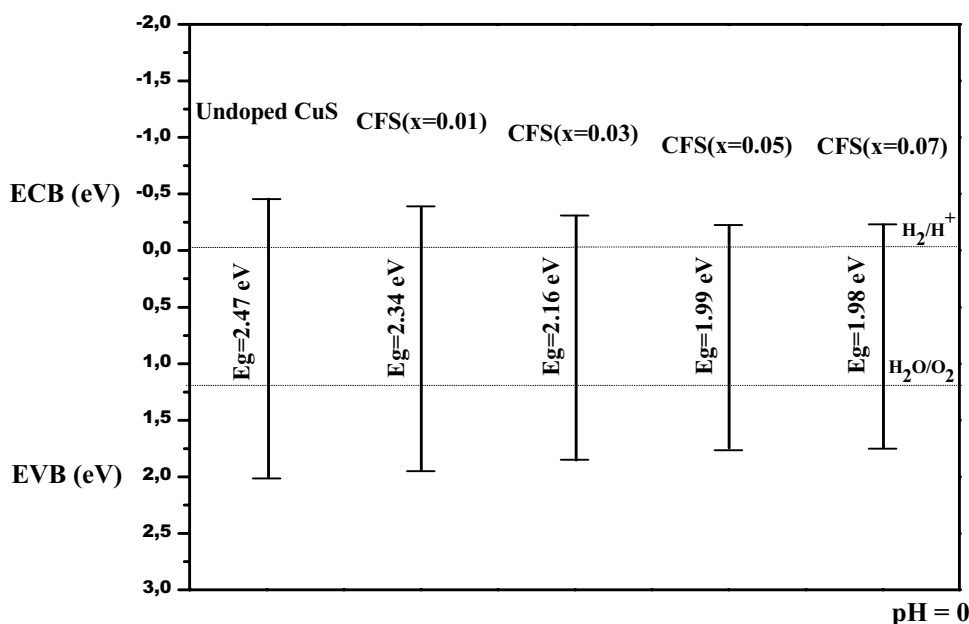


$1.712 \times 10^5 \text{ cm}^{-1}$. For comparison, the absorption coefficient of CuS was $1.155 \times 10^5 \text{ cm}^{-1}$, which is higher than the values obtained previously [59, 60]. There is no report accessible of absorption coefficient for Fe doped CuS. This extended absorption give opportunities to a possible photocatalytic activity enhancement with CFS thin films illuminate by solar irradiation.

4 Photocatalysis properties analysis

It has been found that the band gap value 2.47 eV of CuS is wider than minimum band gap 1.23 eV required for the water splitting reactions, showing the ability of the use of CuS doped Fe for photocatalytic water splitting and hydrogen production using the solar spectrum and the visible light region. Figure 8 shows the different band gap of the CFS thin films according to doping levels, relative to water oxidation

Fig. 8 Calculated band edge positions of undoped and various Fe-doped CuS thin films in comparison with water redox in pH = 0 solutions



and reduction potential standard levels respecting the Normal Hydrogen Electrode (NHE). To produce hydrogen at ambient conditions, the minimum of the CB (maximum of the VB) should locate slower than the Hydrogen reduction potential (0 V vs NHE) and must be located upper than the oxidation potential of O₂/H₂O. The valence and conduction bands edges position can be estimated by : $E_{VB} = E_{CB} + E_g$ with $E_{CB} = X - E_0 - 0.5E_g$ [61] where E_{VB} and E_{CB} are the potential of the valence and conduction bands edges, respectively, E_0 (~ 4.5 eV) is the energy of free electrons on the hydrogen scale, E_g is the band gap energy from our experimental results, and X is the Mulliken electronegativity of CuS and Cu_{1-x}Fe_xS (x = 0.01, 0.03, 0.05 and 0.07) which is calculated about 5.28, 5.28, 5.27, 5.26, and 5.26 eV, respectively; based on atomic ionization energies and electron affinities. We demonstrate that the band edge position is suitable for the water splitting for CuS and Fe doped CuS (Fig. 8), Reason that made from CFS a material with a strong photocatalytic potential. However, the redox potential of the water in the photocatalysis water splitting is dependent strongly on solutions pH value. For CuS and CFS the standard oxidation potentials O₂/H₂O and reduction potentials H⁺/H₂ are given by [62]:

$$E_{O_2/H_2O}^{ox}(CuS) = -0.455 + 0.059 \times pH \text{ eV} \tag{6}$$

$$E_{H^+/H_2}^{red}(CuS) = 2.015 + 0.059 \times pH \text{ eV} \tag{7}$$

$$E_{O_2/H_2O}^{ox}CFS(1 \text{ at}\%) = -0.39 + 0.059 \times pH \text{ eV} \tag{8}$$

$$E_{H^+/H_2}^{red}CFS(1 \text{ at}\%) = 1.95 + 0.059 \times pH \text{ eV} \tag{9}$$

$$E_{O_2/H_2O}^{ox}CFS(3 \text{ at}\%) = -0.31 + 0.059 \times pH \text{ eV} \tag{10}$$

$$E_{H^+/H_2}^{red}CFS(3 \text{ at}\%) = 1.85 + 0.059 \times pH \text{ eV} \tag{11}$$

$$E_{O_2/H_2O}^{ox}CFS(5 \text{ at}\%) = -0.225 + 0.059 \times pH \text{ eV} \tag{12}$$

$$E_{H^+/H_2}^{red}CFS(5 \text{ at}\%) = 1.765 + 0.059 \times pH \text{ eV} \tag{13}$$

$$E_{O_2/H_2O}^{ox}CFS(7 \text{ at}\%) = -0.23 + 0.059 \times pH \text{ eV} \tag{14}$$

$$E_{H^+/H_2}^{red}CFS(7 \text{ at}\%) = 1.75 + 0.059 \times pH \text{ eV} \tag{15}$$

According to the equations, by changing the pH of the solution we can shift the oxidation of water's and reduction potentials, this induce a tune of the band edge alignment of CFS

to be more appropriate to the O₂/H₂O and H⁺/H₂ reduction-oxidation potential by adjusting the ratio between the oxidizing rate (recognized as the H⁺/H₂ and the VB potential difference) and the reducing rate (recognized as the O₂/H₂O and the CB the potential difference), to be equal to 1. For instance, for CuS and CFS, we have showing in Fig. 9, the band position conditions for water splitting (VB positive than H⁺/H₂ potential, plus CB negative than O₂/H₂O potential) are verified : from pH = 0 to 12 for CuS, from pH = 0 to 11 for CFS (x = 0.01), from pH = 0 to 9 for CFS (x = 0.03), from pH = 0 to 8 for CFS (x = 0.05), and for pH = 0 to 7 for CFS (x = 0.07), for pH = 3 solutions, oxidation potential and reduction potential move up to 0.18 V, making the oxidizing rate equal to the reducing one resulting a pleasing conditions for water splitting (Fig. 10), required criteria for a photocatalyst material for water splitting. By this analysis the CFS (x = 0.07) in a solution with pH = 3 could be a promising material for water splitting and both hydrogen-oxygen production. Nevertheless, the CFS (x = 0.01, 0.03, 0.05 and 0.07) compounds can be used with a pH solutions between 7 and 8 to produce hydrogen, by forming heterostructure between CuS and CFS, it can be seen from Table 1 that there is a strong quasi-lattice parameter agreement, result in a good structural tunability. Figure 11 shows the photogenerated electrons in the semiconductor with the greater CB (CuS with $E_{CB} = -0.927$ eV) migrate to the minimum energy conduction band which is that of the semiconductor (CFS (0.07) with $E_{CB} = -0.702$ eV), going through CFS (0.01) with $E_{CB} = -0.862$ eV, CFS (0.03) with $E_{CB} = -0.782$ eV, CFS (0.05) with $E_{CB} = -0.697$ eV. While the photogenerated holes with the lowest VB energy (CFS(0) with $E_{VB} = 1.543$ eV) move to the semiconductor VB which having the highest VB energy (CFS (0.07) with $E_{VB} = 1.278$ eV), going through CFS (1 at%) with $E_{VB} = 1.478$ eV, CFS (0.03) with $E_{VB} = 1.378$ eV, and CFS (0.05) with $E_{VB} = 1.293$ eV, based on the position of the flat bands the semiconductors CuS and CFS create a straddling gap heterostructure type, which ameliorate the power of the reduction and oxidation in photocatalysis.

The major reactions on the surface of the ideal photocatalyst semiconductor Cu_{1-x}Fe_xS (x = 0.07) can be described in Eq. (16), result in two fundamental steps for water splitting Eqs. (17, 18) for hydrogen and oxygen evolution.

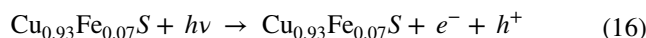


Fig. 9 Calculated band edge positions of undoped and various Fe-doped CuS thin films in comparison with water redox in with variation of the pH solutions

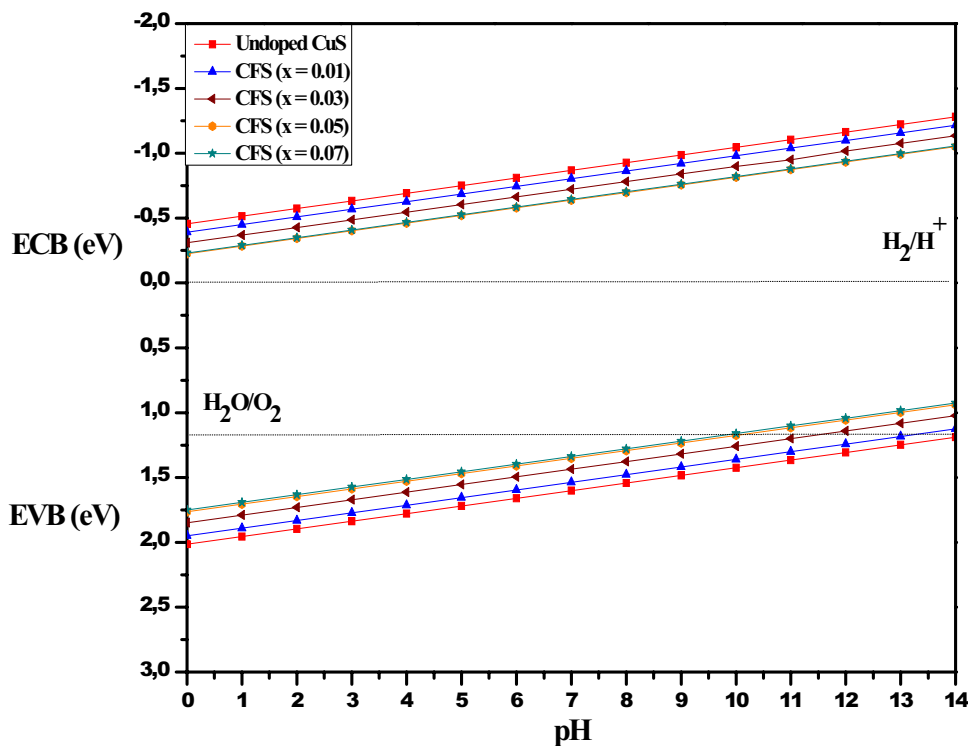
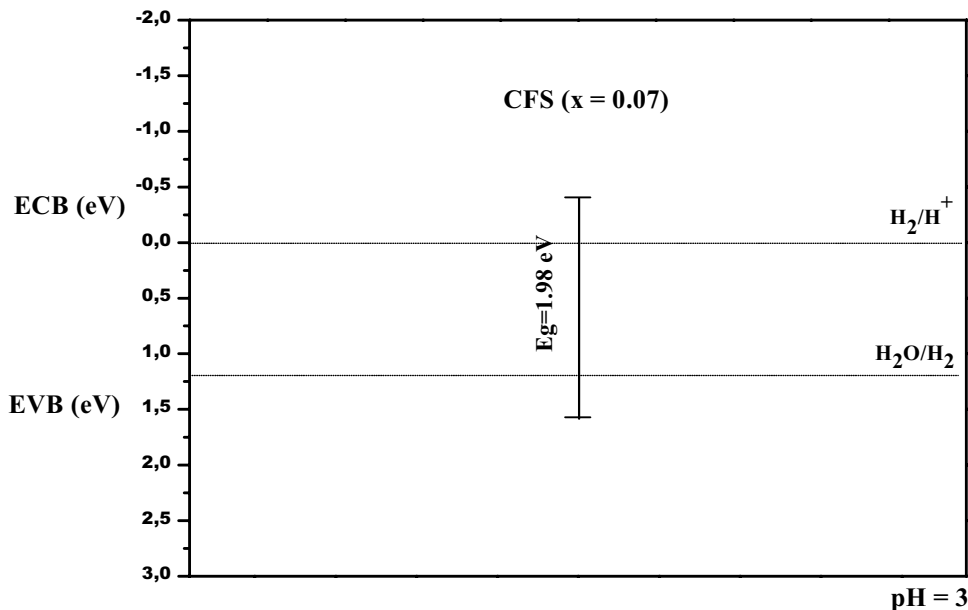


Fig. 10 Calculated band edge positions of CFS (7 at%) in comparison with water redox in with variation pH = 3 solutions

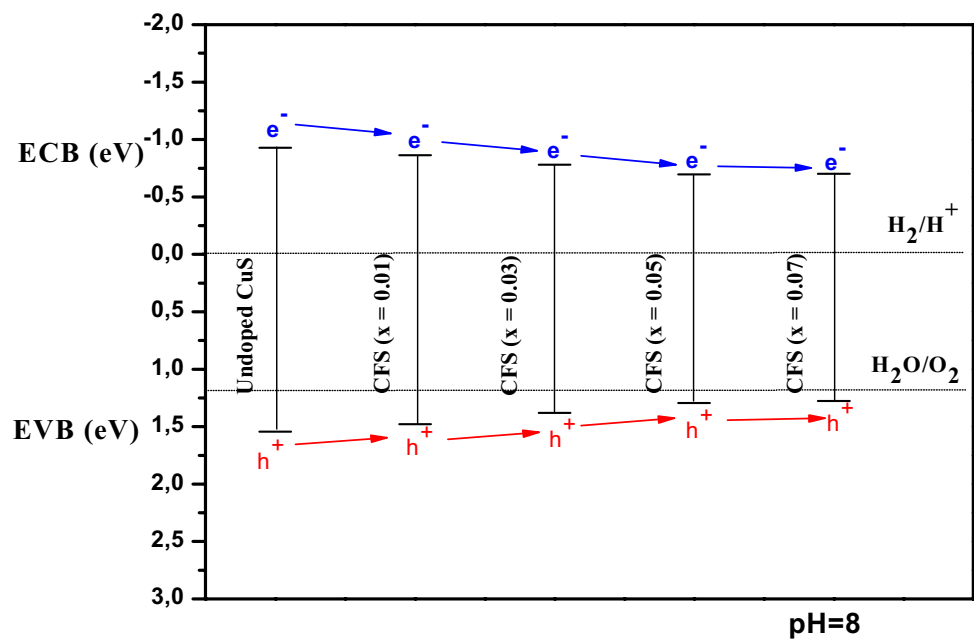


5 Conclusions

In this work, we have studied in detail the structural and optical properties of CuS and Cu_{1-x}Fe_xS (CFS) (*x* = 0.01, 0.03, 0.05 and 0.07) thin film for photocatalysis a possible application, elaborated via the deposition technique Chemical Spray Pyrolysis (CSP). The XRD results demonstrated that the deposited thin films from a Covellite single phase

CuS without formation of other phases. The lattice has a hexagonal structure with dimensions, *a* = *b* = 3.79 Å and *c* = 16.34 Å in accord with the reported lattice parameters. The grain sizes for the CuS and CFS films were in the span of 121–171 Å. The UV–Vis spectrum analysis revealed that the energy band gap was reduced from 2.47 to 1.98 eV and that the film absorption coefficients have improved from 1.155 × 10⁵ to 1.712 × 10⁵ cm⁻¹. For Fe doped CuS, an accurate band gap and band edge alignment with right

Fig. 11 Representation of the straddling gap heterostructure present in a undoped and various Fe-doped CuS thin films heterostructure



pH value boosts the applicability of the material as a photocatalyst for visible light. According to this study, CFS ($x = 0.07$) thin films in pH = 3 solutions is a promising material for photocatalysis application for water splitting to hydrogen–oxygen production. Nevertheless, we demonstrate that the formation of straddling gap heterostructure for CuS and CFS in pH solution between 7 and 8 induce the production of oxygen and hydrogen.

Declarations

Conflict of interest The authors declare that they do not have any conflict of interest.

References

- H.L. Wang, L.S. Zhang, Z.G. Chen, J.Q. Hu, S.J. Li, Z.H. Wang, J.S. Liu, X.C. Wang, Semiconductor heterojunction photocatalysts: design, construction, and photocatalytic performances. *Chem. Soc. Rev.* **43**, 5234–5244 (2014)
- H. Li, J. Shang, Z.H. Ai, L.Z. Zhang, Efficient visible light nitrogen fixation with BiOBr nanosheets of oxygen vacancies on the exposed 001 facets. *J. Am. Chem. Soc.* **137**, 6393–6399 (2015)
- S. Khanchandani, S. Kumar, A.K. Ganguli, Comparative study of TiO₂/CuS core/shell and composite nanostructures for efficient visible light photocatalysis. *ACS. Sustain. Chem. Eng.* **4**, 1487–1499 (2016)
- M.D. Regulacio, M.Y. Han, Multinary I-III-VI₂ and I₂-II-IV-VI₄ semiconductor nanostructures for photocatalytic applications. *Acc. Chem. Res.* **49**, 511–519 (2016)
- A.P. Alivisatos, Semiconductor clusters, nanocrystals, and quantum dots. *Science* **271**, 933–937 (1996)
- G.H. Yue, P.X. Yan, X.Y. Fan, M.X. Wang, D.M. Qu, Z.G. Wu, C. Li, D. Yan, Structure and properties of cobalt disulfide nanowire arrays fabricated by electrodeposition. *Solid State. Lett.* **10**, D29–D31 (2007)
- G.H. Yue, P.X. Yan, X.Y. Fan, M.X. Wang, D.M. Qu, D. Yan, J.Z. Liu, Characterization of the single crystalline iron sulfide nanowire array synthesis by pulsed electrodeposition. *J. Appl. Phys.* **100**, 124313–124316 (2006)
- C. Krataitong, K. Srichai, A. Tubtimtae, Structural and optical properties of undoped and antimony doped lead telluride thin films. *Mater. Lett.* **285**, 129085 (2021)
- Z.H. Wang, D.Y. Geng, Y.J. Zhang, Z.D. Zhang, CuS: Ni flower-like morphologies synthesized by the solvothermal route. *Mater. Chem. Phys.* **122**, 241–245 (2010)
- S.D. Sartale, C.D. Lokhande, Growth of copper sulphide thin films by successive ionic layer adsorption and reaction (SILAR) method. *Mater. Chem. Phys.* **65**, 63 (2000)
- E.C. Greyson, J.E. Barton, T.W. Odom, Tetrahedral zinc blende tin sulfide nano- and microcrystals. *Small.* **2**, 368–371 (2006)
- J.B. Johnson, H. Jones, B.S. Latham, J.D. Parker, R.D. Engelken, C. Barber, Optimization of photoconductivity in vacuum-evaporated tin sulfide thin films. *Semicond. Sci. Technol.* **14**, 501–507 (1999)
- D.J. Milliron, S.M. Hughes, Y. Cui, L. Manna, J.B. Li, L.W. Wang, A.P. Alivisatos, Colloidal nanocrystal heterostructures with linear and branched topology. *Nature.* **430**, 190 (2004)
- N. Sreelekha, K. Subramanyam, D.A. Reddy, G. Murali, K.R. Varma, R.P. Vijayalakshmi, Efficient photocatalytic degradation of rhodamine-B by Fe doped CuS diluted magnetic semiconductor nanoparticles under the simulated sunlight irradiation. *Solid State. Sci.* **62**, 71–81 (2016)
- N. Sreelekha, K. Subramanyam, D.A. Reddy, G. Murali, S. Ramu, K.R. Varma, R.P. Vijayalakshmi, Structural, optical, magnetic and photocatalytic properties of Co doped CuS diluted magnetic semiconductor nanoparticles. *Appl. Surf. Sci.* **378**, 330–340 (2016)
- Y.C. Chen, J.B. Shi, C. Wu, C.J. Chen, Y.T. Lin, P.F. Wu, Fabrication and optical properties of CuS nanowires by sulfuring method. *Mater. Lett.* **62**, 1421 (2008)
- M. Behboudnia, B. Khanbabaee, Investigation of nanocrystalline copper sulfide Cu₇S₄ fabricated by ultrasonic radiation technique. *J. Cryst. Growth.* **304**, 158 (2007)

18. J.S. Chung, H.J. Sohn, Electrochemical behaviors of CuS as a cathode material for lithium secondary batteries. *J. Power Sources* **108**, 226–231 (2002)
19. S. Lindroos, A. Arnold, M. Leskela, Growth of CuS thin films by the successive ionic layer adsorption and reaction method. *Appl. Surf. Sci.* **158**, 75–80 (2000)
20. K.J. Wang, G.D. Li, J.X. Li, Q. Wang, J.S. Chen, Formation of single-crystalline CuS nanoplates vertically standing on flat substrate. *Cryst. Growth Des.* **7**, 2265 (2007)
21. R.S. Mane, C.D. Lokhande, Chemical deposition method for metal chalcogenide thin films. *Mater. Chem. Phys.* **65**, 11–31 (2000)
22. A. Setkus, A. Galdikas, A. Mironas, I. Simkiene, I. Ancutiene, V. Janickis, S. Kaciulis, G. Mattogno, G.M. Ingo, Properties of Cu_xS thin film based structures: influence on the sensitivity to ammonia at room temperatures. *Thin Solid Films* **391**, 275–281 (2001)
23. J. Liu, D.F. Xue, Solvothermal synthesis of CuS semiconductor hollow spheres based on a bubble template route. *J. Cryst. Growth* **311**, 500–503 (2009)
24. X.P. Shen, H. Zhao, H.Q. Shu, H. Zhou, A.H. Yuan, Self-assembly of CuS nanoflakes into flower-like microspheres: synthesis and characterization. *J. Phys. Chem. Solid* **70**, 422–427 (2009)
25. J. Xu, X.J. Cui, J.H. Zhang, H.W. Liang, H.Y. Wang, J.F. Li, Preparation of CuS nanoparticles embedded in poly (vinyl alcohol) nanofibre via electrospinning. *Bull. Mater. Sci.* **31**, 189 (2008)
26. X.S. Du, Z.Z. Yu, A. Dasari, J. Ma, Y.Z. Meng, Y.W. Mai, Facile synthesis and assembly of Cu₂S nanodisks to corncoblike nanostructures. *Chem. Mater.* **18**, 5156 (2006)
27. S.M. Ou, Q. Xie, D.K. Ma, J.B. Liang, X.K. Hu, W.H. Yu, Y.T. Qian, A precursor decomposition route to polycrystalline CuS nanorods. *Chem. Phys.* **94**, 460 (2005)
28. Q. Lu, F. Gao, D. Zhao, One-step synthesis and assembly of copper sulfide nanoparticles to nanowires, nanotubes, and nanovesicles by a simple organic amine-assisted hydrothermal process. *Nano Lett.* **2**, 725 (2002)
29. X.P. Feng, Y.X. Li, H.B. Liu, Y.L. Li, S. Cui, N. Wang, L. Jiang, X.F. Liu, M.J. Yuan, Controlled growth and field emission properties of CuS nanowalls. *Nanotechnol.* **18**, 145706 (2007)
30. I. Puspitasari, T.P. Gujar, K.D. Jung, O.S. Joo, Simple chemical preparation of CuS nanowhiskers. *Mater. Sci. Eng. B.* **140**, 199 (2007)
31. H.T. Zhang, G. Wu, X.H. Chen, Controlled synthesis and characterization of covellite (CuS) nanoflakes. *Mater. Chem. Phys.* **98**, 298 (2006)
32. M. Saranya, A.N. Grace, Hydrothermal synthesis of CuS nanostructures with different morphology. *J. Nano Res.* **18**, 43–51 (2012)
33. Y. Zhao, F. Xiao, and Q. Jiao. (2011) Hydrothermal synthesis of Ni/Al layered double hydroxide nanorods. *J. Nanotechnol.* Article ID 646409, 6 pages
34. M. Saranya, G. Srishti, S. Iksha, R. Ramachandran, C. Santhosh, C. Harish, T.V. Mudaliar, C.M. Bhanu, G.A. Nirmala, Solvothermal preparation of ZnO/graphenenanocomposites and its photocatalytic properties. *Nanosci. Nanotechnol. Lett.* **5**, 349–354 (2013)
35. P. Roy, S.K. Srivastava, Solvothermal growth of flowerlike morphology from nanorods of copper sulfides. *J. Nanosci. Nanotechnol.* **8**, 1523–1527 (2008)
36. Y.B. Chen, L. Chen, L.M. Wu, Water-induced thermolytic formation of homogeneous core-shell CuS microspheres and their shape retention on desulfurization. *Cryst. Growth Des.* **8**, 2736–2740 (2008)
37. P. Roy, K. Mondal, S.K. Srivastava, Synthesis of twinned CuS nanorods by a simple wet chemical method. *Cryst. Growth Des.* **8**, 1530–1534 (2008)
38. L. Reijnen, B. Meester, F. De Lange, J. Schoonman, A. Goossens, Comparison of Cu-S films grown by atomic layer deposition and chemical vapor deposition. *Chem. Mater.* **17**, 2724–2728 (2005)
39. P. Roy, S.K. Srivastava, Low-temperature synthesis of CuS nanorods by simple wet chemical method. *Mater. Lett.* **61**, 1693–1697 (2007)
40. M. Adelifard, H. Eshghi, M. Mehdi, B. Mohagheghi, An investigation on substrate temperature and copper to sulphur molar ratios on optical and electrical properties of nanostructural CuS thin films prepared by spray pyrolysis method. *Appl. Surf. Sci.* **258**, 5733 (2012)
41. M.A. Yildirim, A. Ates, A. Astam, Annealing and light effect on structural, optical and electrical properties of CuS CuZnS and ZnS thin films grown by the SILAR method. *Physica. E.* **41**, 1365–1372 (2009)
42. R. Suárez, P.K. Nair, Co-deposition of PbS–CuS thin films by chemical bath technique. *J. Solid State. Chem.* **123**, 296–300 (1996)
43. K. Subramanyam, N. Sreelekha, D.A. Reddy, G. Murali, K.R. Varma, R.P. Vijayalakshmi, Chemical synthesis, structural, optical, magnetic characteristics and enhanced visible light active photocatalysis of Ni doped CuS nanoparticles. *Solid State. Sci.* **65**, 68–78 (2017)
44. S.A. Wolf, D.D. Awschalom, R.A. Buhrman, J.M. Daughton, S. Von Molnar, M.L. Roukes, A.Y. Chtchelkanova, D.M. Treger, Spintronics: a spin-based electronics vision for the future. *Science* **294**, 1488–1495 (2001)
45. K. Sato, H.K. Yoshida, Hyperfine interactions and magnetism of 3d transition metal-impurities in II–VI and III–V compound-based diluted magnetic semiconductors. *Hyperfine. Interact.* **136**, 737–742 (2001)
46. M. Rouchdi, E. Salmani, N. Hassanain, A. Mzerd, Effect of deposition time on structural and physical properties of Cu₂CdSnS₄ thin films prepared by spray pyrolysis technique: experimental and ab initio study. *Opt. Quantum. Electron.* **49**, 165–176 (2017)
47. M. Rouchdi, E. Salmani, H. Cherrad, M. Addou, H. Ez-zahraouy, N. Hassanain, A. Mzerd, Spray pyrolysis synthesis of Cu_xFe_{1-x}S₂ and their structural, electronic and optical properties: Experimental and first-principles study. *Mater. Sci. Eng.* **227**, 100–109 (2018)
48. M. Rouchdi, E. Salmani, C. Nassiri, A.E. Hat, N. Hassanain, A. Mzerd, Synthesis and magnetic properties of Mg doped SnO₂ thin films: experimental and Ab-initio study. *Opt. Quantum. Electron.* **49**, 150–162 (2017)
49. M. Rouchdi, E. Salmani, A.E. Hat, N. Hassanain, A. Mzerd, Synthesis and magnetic properties of Ni doped ZnO thin films: experimental and Ab-initio study. *Surf. Rev. Lett.* **7**, 1750085–1750094 (2017)
50. M. Rouchdi, E. Salmani, B. Fares, N. Hassanain, A. Mzerd, Synthesis and characteristics of Mg doped ZnO thin films: experimental and ab initio study. *Results. Phys.* **7**, 620–627 (2017)
51. M. Rouchdi, N. Hassanain, E. Salmani, and A. Mzerd. 2016 Effect of Gd doping and (Gd, Li) co-doping ZnO thin films on optical properties: Experimental and ab-initio study, in *Renewable and Sustainable Energy Conference (IRSEC)*, IEEE (2016), pp. 17–22
52. F.D. Paraguay, J. Morales, W.L. Estrada, E. Andrade, M.M. Yoshida, Influence of Al, In, Cu, Fe and Sn dopants in the microstructure of zinc oxide thin films obtained by spray pyrolysis. *Thin Solid Films* **366**, 16–27 (2000)
53. S. Mustapha, M.M. Ndamitso, A.S. Abdulkareem, J.O. Tijani, D.T. Shuaib, A.K. Mohammed, A. Sumaila, Comparative study of crystallite size using Williamson-Hall and Debye-Scherrer plots for ZnO nanoparticles. *Adv. Nat. Sci. Nanosci. Nanotechnol.* **10**, 045013 (2019)
54. S.M. Londoño-Restrepo, R. Jeronimo-Cruz, B.M. Millán-Malo, E.M. Rivera-Muñoz, M.E. Rodríguez-García, Effect of the

- nano crystal size on the X-ray diffraction patterns of biogenic hydroxyapatite from human, bovine, and porcine bones. *Scientific Rep.* **9**, 1–12 (2019)
55. J. Markmann, V. Yamakov, J. Weissmüller, Validating grain size analysis from X-ray line broadening: a virtual experiment. *Scripta Materialia* **59**, 15–18 (2008)
56. Y. Zhang, J. Tian, H. Li, L. Wang, X. Qin, A.M. Asiri, A.O. Al-Youbi, X. Sun, Biomolecule assisted, environmentally friendly, one-pot Synthesis of CuS/reduced graphene oxide nanocomposites with enhanced photocatalytic performance. *Langmuir*. **28**, 12893–12900 (2012)
57. A.M. Qin, Y.P. Fang, H.D. Ou, H. Liu, C.Y. Su, Formation of various morphologies of covellite copper sulfide submicron crystals by a hydrothermal method without surfactant. *Cryst. Growth Des.* **5**, 855–860 (2005)
58. Q. Yu, S. Cai, Z. Jin, Z. Yan, Evolutions of composition, microstructure and optical properties of Mn-doped pyrite (FeS₂) films prepared by chemical bath deposition. *Mater. Res. Bull.* **48**, 3601–3606 (2013)
59. T. Hurma, S. Kose, XRD Raman analysis and optical properties of CuS nanostructured film. *Optik*. **127**, 6000–6006 (2016)
60. M. Adelifard, H. Eshghi, M.M.B. Mohagheghi, An investigation on substrate temperature and copper to sulphur molar ratios on optical and electrical properties of nanostructural CuS thin films prepared by spray pyrolysis method. *Appl. Surf. Sci.* **258**, 5733–5738 (2012)
61. M. Long, W. Cai, J. Cai, B. Zhou, X. Chai, Y. Wu, Efficient photocatalytic degradation of phenol over Co₃O₄/BiVO₄ composite under visible light irradiation. *J. Phys. Chem. B.* **110**, 20211–20216 (2006)
62. V. Chakrapani, J.C. Angus, A.B. Anderson, S.D. Wolter, B.R. Stoner, G.U. Sumanasekera, Charge transfer equilibria between diamond and an aqueous oxygen electrochemical redox couple. *Science* **318**(5855), 1424–1430 (2007)

Publisher's Note Springer Nature remains neutral with regard to jurisdictional claims in published maps and institutional affiliations.